Mathematical Modeling of the Intervertebral Disc as an Infrastructure for Studying the Mechanobiology of the Tissue Engineering Procedure

MOHAMMAD HAGHPANAHI [a], MOHAMMAD NIKKHOO [a], HABIBALLAH PEIROVI [b],
JALAL-EDIN GHANAVI [c]

[a] Department of Mechanical Engineering
Iran University of Science and Technology
IUST St., Hengam Ave., Resalat Square,Tehran
IRAN
mhaghpanahi@iust.ac.ir, mnikkhoo@mecheng.iust.ac.ir

[b] Nanomedicine and Tissue Engineering Research Center
Shaheed Beheshti University of Medical Science and Health Services
Taleghani Hospital, Velenjak, Tehran
IRAN
peirovi@sbmu.ac.ir

[c] National Research Institute of Tuberculosis and Lung Diseases
Shaheed Beheshti University of Medical Science and Health Services
Darabad, Shaheed Bahonar Ave., Tehran
IRAN
ghanavi@sbmu.ac.ir

Abstract: - Mechanical stress has a significant influence on the residing cells in the intervertebral disc and we can nominate it as one of the principle fields of researches in tissue engineering. So it is very important to propose a suitable model as an infrastructure for a better understanding of the mechanobiology of the intervertebral disc. This paper presents a novel finite element formulation which can be used in our predicted tissue engineering procedure as a powerful model. After derivation of the governmental equations, the standard Galerkin weighted residual method was used to form the finite element model. Then the implicit time integration schemes were applied to solve the nonlinear equations. The formulation accuracy and convergence for 1D case were examined with Sun's and Simon's analytical solution and also Drost's experimental Data. It is shown that the mathematical model is in excellent agreement and has the capability to simulate the intervertebral disc response under different types of mechanical and electrochemical loading conditions. At the end, to have a short review of the capability of the model, three main exemplary problems are proposed. So in this case, investigation of the role of porosity in scaffold manufacturing, effect of FCD and water content on mechanical response and also the nutrition criterion in IVD tissue engineering procedure are discussed.

Key-Words: - Finite element modeling, Porous media, Intervertebral disc, Mechanobiology, Tissue engineering

1 Introduction

Low back pain, which is often caused by disc degeneration, is a major health problem [1, 2]. Current treatment modalities involve conservative management (medication and physical therapy) or surgical intervention (spine fusion, total disc replacement, or nucleus pulposus replacement) [3, 4]. Due to the limitations of the mentioned treatments for degenerative disc disease, tissue engineering methods to repair the diseased disc have been proposed. One of the major challenges in intervertebral disc tissue engineering is to recreate, in vitro, the physiological environment for optimal culturing of cells seeded in scaffolds constructs [5]. According to the important influence of the mechanical stress on the residing cells in the intervertebral disc, it is vital to propose a suitable mechanical model as an infrastructure for a better understanding of the mechanical behavior of this soft tissue [6, 7].

In general, intervertebral disc is basically formed from a fibrous network of structure proteins,

abundant interstitial water, soluble electrolytes, and cells residing in the interstitial space [8]. So it can be described as a charged, hydrated and permeable material which is comprised largely of collagen and elastic fibers embedded in a proteoglycan gel to form a solid matrix. During the last decade, several researches have been proposed the multiphasic computational models to study mechanics of the soft tissues (such as articular cartilage, intervertebral disc, vascular vessel and skin). Mow et al. [9] first presented the biphasic theory in which the material was modeled as a mixture of two distinct phases and later it was extended by Suh et al. [10-13]. On the basis of the Biot theorem, Simon et al. [14, 15] considered the soft tissues in the spinal motion segment as poroelastic material which was later extended by Yang et al. [16]. Since significant deformations resulting from loading and inherent swelling mechanisms in the soft tissues have been described, Lai et al. [17] developed a triphasic model to consider the effects of swelling and transport in descriptions of soft tissue mechanics. Then Gu et al. [18] and Sun et al. [19] extended triphasic theory to model the mechano-electrochemical behaviors of charged hydrated soft tissues containing electrolytes. Later, Simon et al. [20, 21] and Laible et al. [22, 23] extended poroelastic model to poroelastic transport swelling model which includes chemical effects.

It is so clear that all these models tried to incorporate the features of actual biological tissue but there are some limitations that should be improved for better understanding of the intervertebral disc biomechanics. Except for the model of Simon [14, 15] and Yang [16], the previous models are quasi static which means that the inertia is ignored. Actually, the inertia terms can be significant when the external forces vary rapidly. Additionally, some limited models considered the chemical and electrical effects (Sun [19], Simon [20, 21] and Iatridis [23]), which is so important for us in our predicted tissue engineering procedure. So based on the work of Sun, Simon and Yang, this paper presents a novel mixed finite element formulation including the chemical behaviour and inertia terms which can simulate intervertebral disc response regarding to the different types of mechanical, electrical and physicochemical loading conditions.

2 Mathematical Model

This mathematical model considers a charged hydrated tissue engineered intervertebral disc as a mixture consisting of: (1) a porous, permeable, charged solid phase; (2) an incompressible fluid phase; and (3) ion phase with two ion species, i.e., anion and cation (Fig. 1).
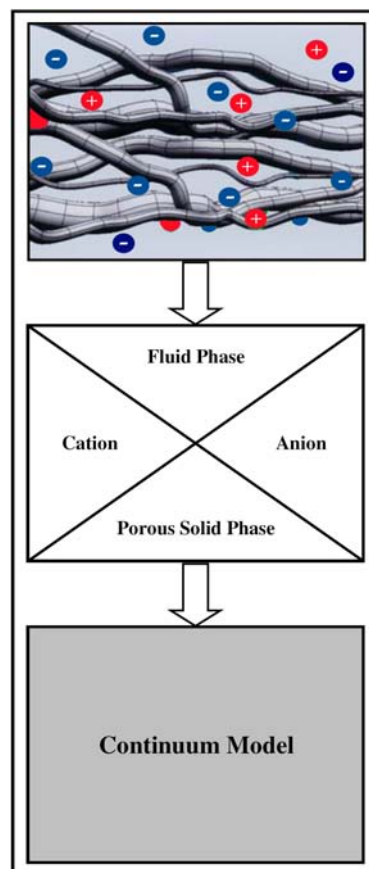

Fig.1: Schematic diagram of the triphasic model of the intervertebral disc (Solid/ Fluid/ Ions)

According to the Biot theory, derivation of the governing equation of the fluid was based on empirical evidence that the fluid flow in porous media obeys Darcy's law [21]. By the way, this model is strictly based on the laws of continuum mechanics [24].

2.1 Porous Model

There are different forces on the solid phase which are the frictional force between solid and fluid, body force, fluid pressure and the pressure due to the chemical potential. So the momentum conservation law for the porous solid in the absence of body force can be written as Eq.1 (More details are mentioned in appendix).

$$\frac{\partial T_{ji}}{\partial X_j} - \rho_s \ddot{u}_i - n\rho_f (J^{-1} \frac{\partial x_i}{\partial X_j})\ddot{w}_j = 0 \qquad (1)$$

As the model satisfies the Darcy equation, the momentum conservation laws for the pore fluid in

the absence of body force can be written as Eq.2 (More details are mentioned in appendix).

$$\frac{\partial(p+\frac{p^c}{n})}{\partial X_i} - \frac{n}{k}\dot{w}_j - \rho_f \frac{\partial x_j}{\partial X_i}\ddot{u}_j$$
$$- \rho_f(J^{-1}\frac{\partial x_k}{\partial X_i}\frac{\partial x_k}{\partial X_j})\ddot{w}_j = 0 \tag{2}$$

Where p^c can be described as Eq.3,

$$p^c = B_f\zeta_w - \rho_f\mu_0 + RT\phi(2c + FCD) \tag{3}$$

The storage due to compressibility of the solid and of the fluid should be equal to the dilation of the fluid and of the solid (On the basis of the mass conservation law). So the fluid pressure can be expressed as Eq.4 [14].

$$p = nQw_{i,i} + \alpha QJ[\frac{\partial X_r}{\partial x_k}E_{rs}\frac{\partial X_s}{\partial x_k}] \tag{4}$$

Where: Q and α are as Eqs.5 and 6.

$$\frac{1}{Q} = \frac{n}{K_{fluid}} + \frac{\alpha - n}{K_{Solid}} \tag{5}$$

$$\alpha = 1 - \frac{K}{K_{solid}} \tag{6}$$

2.2 Electrochemical Model

On the basis of Sun's work [19] (in the absence of the magnetic and gravitational effects), the governmental equations can be derived from the momentum equations, continuity equations and electrical current condition as Eqs.7 and 8.

$$\nabla \cdot \mathbf{J}^+ - \nabla \cdot \mathbf{J}^- = 0 \tag{7}$$

$$\frac{\partial c^k}{\partial t} + \nabla \cdot \mathbf{J}^+ + \nabla \cdot \mathbf{J}^- + \nabla \cdot (c^k \mathbf{v}^s) = 0 \tag{8}$$

Where,

$$\mathbf{J}^+ = -\frac{\rho^+ c^+ \nabla\tilde{\mu}^+(f_{-sf} + f_{-+}) + \rho^- c^+ \nabla\tilde{\mu}^- f_{+-}}{f_{+sf}f_{-sf} + f_{+sf}f_{-+} + f_{+-}f_{-sf}} \tag{9}$$

$$\mathbf{J}^- = -\frac{\rho^- c^- \nabla\tilde{\mu}^-(f_{+sf} + f_{+-}) + \rho^+ c^- \nabla\tilde{\mu}^+ f_{-+}}{f_{+sf}f_{-sf} + f_{+sf}f_{-+} + f_{+-}f_{-sf}} \tag{10}$$

We can rewrite the Eqs.9 and 10 in Eqs.11 and 12 by nominating k_β^α as Eqs.13-16

$$\mathbf{J}^+ = k_1^+ c^+ \nabla\tilde{\mu}^+ + k_2^+ c^+ \nabla\tilde{\mu}^- \tag{11}$$

$$\mathbf{J}^- = k_1^- c^- \nabla\tilde{\mu}^- + k_2^- c^- \nabla\tilde{\mu}^+ \tag{12}$$

$$k_1^+ = -\frac{\rho^+(f_{-sf} + f_{-+})}{f_{+sf}f_{-sf} + f_{+sf}f_{-+} + f_{+-}f_{-sf}} \tag{13}$$

$$k_2^+ = -\frac{\rho^- f_{+-}}{f_{+sf}f_{-sf} + f_{+sf}f_{-+} + f_{+-}f_{-sf}} \tag{14}$$

$$k_1^- = -\frac{\rho^-(f_{+sf} + f_{+-})}{f_{+sf}f_{-sf} + f_{+sf}f_{-+} + f_{+-}f_{-sf}} \tag{15}$$

$$k_2^- = -\frac{\rho^+ f_{-+}}{f_{+sf}f_{-sf} + f_{+sf}f_{-+} + f_{+-}f_{-sf}} \tag{16}$$

3 FE Formulation of the Model

Using the standard Galerkin weighted residual method [25], the finite element formulation is constructed [24].

Multiply the Eqs.1, 2, 4, 7 and 8 by the weight function W, and integrating over the domain of the problem, gives Eqs.17-21.

$$\int_\Omega \mathbf{W}(\frac{\partial T_{ji}}{\partial X_j} - \rho\ddot{u}_i - n\rho_f(J^{-1}\frac{\partial x_i}{\partial X_j})\ddot{w}_j)d\Omega = 0 \tag{17}$$

$$\int_\Omega \mathbf{W}\left(\begin{array}{c}\dfrac{\partial(p+\frac{p^c}{n})}{\partial X_i} - \dfrac{n}{k}\dot{w}_j - \rho_f\dfrac{\partial x_j}{\partial X_i}\ddot{u}_j \\ - \rho_f(J^{-1}\dfrac{\partial x_k}{\partial X_i}\dfrac{\partial x_k}{\partial X_j})\ddot{w}_j\end{array}\right)d\Omega = 0 \tag{18}$$

$$\int_\Omega \mathbf{W}\left(p - nQw_{i,i} + \alpha QJ[\frac{\partial X_r}{\partial x_k}E_{rs}\frac{\partial X_s}{\partial x_k}]\right)d\Omega = 0 \tag{19}$$

$$\int_\Omega \mathbf{W}(\nabla \cdot \mathbf{J}^+ - \nabla \cdot \mathbf{J}^-) = 0 \tag{20}$$

$$\int_\Omega \mathbf{W}(\frac{\partial c^k}{\partial t} + \nabla \cdot \mathbf{J}^+ + \nabla \cdot \mathbf{J}^- + \nabla \cdot (c^k \mathbf{v}^s))d\Omega = 0 \tag{21}$$

Choosing the shape functions as the weight functions, separating the integrals, applying Green's theorem for Eqs.17 and 19 and also divergence theorem for Eq.21, yields:

$$\int_\Omega N_{mi,j}^u T_{ji}d\Omega + (\int_\Omega \rho N_{mi}^u N_{ni}^u d\Omega)\ddot{u}_{ni}$$
$$- \int_{\partial\Omega} N_{mi}^u t_i ds \tag{22}$$
$$+ (\int_\Omega N_{mi}^u n\rho_f(J^{-1}\frac{\partial x_i}{\partial X_j})N_{nj}^w d\Omega)\ddot{w}_{nj} = 0$$

$$\int_\Omega N_{mi}^w N_{n,i}^w p_n d\Omega + \int_\Omega N_{mi}^w \frac{p^c,i}{n} d\Omega$$

$$- \int_\Omega \frac{n}{k} N_{mi}^w N_{ni}^w d\Omega \dot{w}_{nj} - \int_\Omega N_{mi}^w \rho_f \frac{\partial x_j}{\partial X_i} N_{nj}^w d\Omega \ddot{u}_{nj} \qquad (23)$$

$$- \int_\Omega N_{mi}^w \frac{\rho_f}{J} \frac{\partial x_k}{\partial X_i} \frac{\partial x_k}{\partial X_j} N_{ni}^w d\Omega \ddot{w}_{nj} = 0$$

$$\int_\Omega N_m^p N_n^p d\Omega p$$

$$- \int_\Omega (nQw_{i,i} + \alpha QJ[\frac{\partial X_r}{\partial x_k} E_{rs} \frac{\partial X_s}{\partial x_k}])_n N_m^p d\Omega = 0 \qquad (24)$$

$$\int_\Omega \begin{matrix} (k_1^+ c^+ \nabla \tilde{\mu}^+ N^c + k_2^+ c^+ \nabla \tilde{\mu}^- N^c \\ - k_1^- c^- \nabla \tilde{\mu}^- N^c - k_2^- c^- \nabla \tilde{\mu}^+ N^c).\mathbf{n} \end{matrix} ds$$

$$+ \int_\Omega (-k_1^+ c^+ + k_2^- c^-)(\nabla N^c) \cdot (\nabla N^c) d\Omega \cdot \tilde{\mu}^+ \qquad (25)$$

$$+ \int_\Omega (-k_2^+ c^+ + k_1^- c^-)(\nabla N^c) \cdot (\nabla N^c) d\Omega \cdot \tilde{\mu}^- = 0$$

$$\int_\Omega N^c (\frac{\partial c^k}{\partial t}) d\Omega$$

$$+ \int_\Omega \begin{matrix} (k_1^+ c^+ \nabla \tilde{\mu}^+ N^c + k_2^+ c^+ \nabla \tilde{\mu}^- N^c \\ + k_1^- c^- \nabla \tilde{\mu}^- N^c + k_2^- c^- \nabla \tilde{\mu}^+ N^c).\mathbf{n} \end{matrix} ds$$

$$- \int_\Omega (k_1^+ c^+ + k_2^- c^-)(\nabla N^c) \cdot (\nabla N^c) d\Omega \cdot \tilde{\mu}^+ \qquad (26)$$

$$- \int_\Omega (k_2^+ c^+ + k_1^- c^-)(\nabla N^c) \cdot (\nabla N^c) d\Omega \cdot \tilde{\mu}^-$$

$$+ \int_s (c^k \mathbf{v}^s N^c) \cdot \mathbf{n} ds - \int_\Omega (\nabla N^c) \cdot (c^k \mathbf{v}^s) d\Omega = 0$$

So finally, Eqs.22-26 can be classified in matrix form as Eqs.27-29.

$$\begin{bmatrix} \mathbf{M_{11}} & \mathbf{M_{12}} & \mathbf{0} \\ \mathbf{M_{21}} & \mathbf{M_{22}} & \mathbf{0} \\ \mathbf{0} & \mathbf{0} & \mathbf{0} \end{bmatrix} \begin{bmatrix} \ddot{\mathbf{u}} \\ \ddot{\mathbf{w}} \\ \ddot{\mathbf{p}} \end{bmatrix} + \begin{bmatrix} \mathbf{0} & \mathbf{0} & \mathbf{0} \\ \mathbf{0} & \mathbf{C_{22}} & \mathbf{0} \\ \mathbf{0} & \mathbf{0} & \mathbf{0} \end{bmatrix} \begin{bmatrix} \dot{\mathbf{u}} \\ \dot{\mathbf{w}} \\ \dot{\mathbf{p}} \end{bmatrix} = \begin{bmatrix} \mathbf{f_1} \\ \mathbf{f_2} \\ \mathbf{f_3} \end{bmatrix} \qquad (27)$$

$$\mathbf{K}^+ \tilde{\boldsymbol{\mu}}^+ + \mathbf{K}^- \tilde{\boldsymbol{\mu}}^- = \mathbf{f_4} \qquad (28)$$

$$\mathbf{C^c} \dot{\mathbf{c}} = \mathbf{f_5} \qquad (29)$$

Where, the mentioned parameters are defined according to the Eqs.30-42.

$$\mathbf{M_{11}} = \int_\Omega \rho_s N_{mi}^u N_{ni}^u d\Omega \qquad (30)$$

$$\mathbf{M_{12}} = \int_\Omega N_{mi}^u n \rho_f (J^{-1} \frac{\partial x_i}{\partial X_j}) N_{nj}^w d\Omega \qquad (31)$$

$$\mathbf{M_{21}} = \int_\Omega N_{mi}^w \rho_f \frac{\partial x_j}{\partial X_i} N_{nj}^w d\Omega \qquad (32)$$

$$\mathbf{M_{22}} = \int_\Omega N_{mi}^w \frac{\rho_f}{J} \frac{\partial x_k}{\partial X_i} \frac{\partial x_k}{\partial X_j} N_{nj}^w d\Omega \qquad (33)$$

$$\mathbf{C_{22}} = \int_\Omega \frac{n}{k} N_{mi}^w N_{ni}^w d\Omega \qquad (34)$$

$$\mathbf{f_1} = \int_{\partial\Omega} N_{mi}^u t_i ds - \int_\Omega N_{mi,j}^{u^T} \mathbf{T} d\Omega \qquad (35)$$

$$\mathbf{f_2} = \int_\Omega N_{mi}^w N_{n,i}^w \cdot p_n d\Omega + \int_\Omega N_{mi}^w \frac{p^c,i}{n} \cdot d\Omega \qquad (36)$$

$$\mathbf{f_3} = \int_\Omega N_m^p N_n^p d\Omega p - \int_\Omega (nQw_{i,i} + \alpha QJ[\frac{\partial X_r}{\partial x_k} E_{rs} \frac{\partial X_s}{\partial x_k}])_n N_m^p d\Omega \qquad (37)$$

$$\mathbf{K}^+ = \int_\Omega (-k_1^+ c^+ + k_2^- c^-)(\nabla N^c) \cdot (\nabla N^c) d\Omega \qquad (38)$$

$$\mathbf{K}^- = \int_\Omega (-k_2^+ c^+ + k_1^- c^-)(\nabla N^c) \cdot (\nabla N^c) d\Omega \qquad (39)$$

$$\mathbf{f_4} = -\int_\Omega \begin{matrix} (k_1^+ c^+ \nabla \tilde{\mu}^+ N^c + k_2^+ c^+ \nabla \tilde{\mu}^- N^c \\ - k_1^- c^- \nabla \tilde{\mu}^- N^c - k_2^- c^- \nabla \tilde{\mu}^+ N^c).\mathbf{n} ds \end{matrix} \qquad (40)$$

$$\mathbf{C^c} = \int_\Omega N^{c^T} N^c d\Omega \qquad (41)$$

$$\mathbf{f_5} = -\int_\Omega \begin{matrix} (k_1^+ c^+ \nabla \tilde{\mu}^+ N^c + k_2^+ c^+ \nabla \tilde{\mu}^- N^c \\ + k_1^- c^- \nabla \tilde{\mu}^- N^c + k_2^- c^- \nabla \tilde{\mu}^+ N^c).\mathbf{n} ds \end{matrix}$$

$$+ \int_\Omega (k_1^+ c^+ + k_2^- c^-)(\nabla N^c) \cdot (\nabla N^c) d\Omega \cdot \tilde{\mu}^+ \qquad (42)$$

$$+ \int_\Omega (k_2^+ c^+ + k_1^- c^-)(\nabla N^c) \cdot (\nabla N^c) d\Omega \cdot \tilde{\mu}^-$$

$$- \int_s (c^k \mathbf{v}^s N^c) \cdot \mathbf{n} ds + \int_\Omega (\nabla N^c) \cdot (c^k \mathbf{v}^s) d\Omega$$

4 Numerical Solution

The implicit Newmark integration scheme [25, 26] was applied to solve Eq.27. In this method assumptions are as Eqs.43 and 44.

$$^{t+\Delta t}\dot{\mathbf{X}} = ^t\dot{\mathbf{X}} + [(1-\delta)^t\ddot{\mathbf{X}} + \delta^{t+\Delta t}\ddot{\mathbf{X}}]\Delta t \qquad (43)$$

$$^{t+\Delta t}\mathbf{X} = ^t\mathbf{X} + ^t\dot{\mathbf{X}}\Delta t + [(\frac{1}{2} - \alpha)^t\ddot{\mathbf{X}} + \alpha^{t+\Delta t}\ddot{\mathbf{X}}]\Delta t^2 \qquad (44)$$

Where α and δ are parameters that can be determined to obtain integration accuracy and stability. A very common technique used is the trapezoidal rule, which is Newmark method with $\delta = \frac{1}{2}$ and $\alpha = \frac{1}{4}$, and we used this method to demonstrate the basic additional consideration involved in a nonlinear analysis.

So we can rewrite the Eqs.43 and 44 as Eqs.45 and 46,

$$^{t+\Delta t}\dot{\mathbf{X}} = {}^{t}\dot{\mathbf{X}} + \frac{1}{2}[^{t}\ddot{\mathbf{X}} + {}^{t+\Delta t}\ddot{\mathbf{X}}]\Delta t \tag{45}$$

$$^{t+\Delta t}\mathbf{X} = {}^{t}\mathbf{X} + {}^{t}\dot{\mathbf{X}}\Delta t + \frac{1}{4}[^{t}\ddot{\mathbf{X}} + {}^{t+\Delta t}\ddot{\mathbf{X}}]\Delta t^{2} \tag{46}$$

At time $t+\Delta t$, we can write Eq.47 for a dynamic system.

$$\mathbf{M}^{\,t+\Delta t}\ddot{\mathbf{X}} + \mathbf{C}^{\,t+\Delta t}\dot{\mathbf{X}} = {}^{t+\Delta t}\mathbf{F} \tag{47}$$

Elimination $^{t+\Delta t}\ddot{\mathbf{X}}$ and $^{t+\Delta t}\dot{\mathbf{X}}$ by using Eqs.45 to 47, gives Eq.48

$$[\frac{4}{\Delta t^{2}}\mathbf{M} + \frac{2}{\Delta t}\mathbf{C}]^{t+\Delta t}\mathbf{X} = {}^{t+\Delta t}\mathbf{F}$$
$$+ [\frac{4}{\Delta t^{2}}{}^{t}\mathbf{X} + \frac{4}{\Delta t}{}^{t}\dot{\mathbf{X}} + {}^{t}\ddot{\mathbf{X}}]\mathbf{M} + [\frac{2}{\Delta t}{}^{t}\mathbf{X} + {}^{t}\dot{\mathbf{X}}]\mathbf{C} \tag{48}$$

So the term $^{t+\Delta t}\dot{\mathbf{X}}$ and $^{t+\Delta t}\ddot{\mathbf{X}}$ can be updated as Eq.49 and 50.

$$^{t+\Delta t}\dot{\mathbf{X}} = \frac{2}{\Delta t}(^{t+\Delta t}\mathbf{X} - {}^{t}\mathbf{X}) - {}^{t}\dot{\mathbf{X}} \tag{49}$$

$$^{t+\Delta t}\ddot{\mathbf{X}} = \frac{4}{\Delta t^{2}}(^{t+\Delta t}\mathbf{X} - {}^{t}\mathbf{X} - \Delta t\,{}^{t}\dot{\mathbf{X}}) - {}^{t}\ddot{\mathbf{X}} \tag{50}$$

It is clear that $^{t}\dot{\mathbf{X}}$ and $^{t}\ddot{\mathbf{X}}$ are known from the previous step of the calculations. So if $^{t+\Delta t}\mathbf{X}$ is determined from Eq.48, $^{t+\Delta t}\dot{\mathbf{X}}$ and $^{t+\Delta t}\ddot{\mathbf{X}}$ can be obtained from equations 49 and 50. So, the main point of this problem is to solve Eq.48. The Newton method was used for solving Eq.48.

The implicit backward-Euler method [25, 26] was applied to solve Eqs.28 and 29. This method approximates the derivative as Eqs.51

$$^{t+\Delta t}\dot{X} = \frac{1}{\Delta t}(^{t+\Delta t}X - {}^{(t)}X) \tag{51}$$

So Eqs.28 and 29 become as Eqs.52 and 53,

$$^{(t+\Delta t)}\mathbf{K}^{+}\,{}^{(t+\Delta t)}\tilde{\boldsymbol{\mu}}^{+} + {}^{(t+\Delta t)}\mathbf{K}^{-}\,{}^{(t+\Delta t)}\tilde{\boldsymbol{\mu}}^{-} = {}^{(t+\Delta t)}\mathbf{f}_{4} \tag{52}$$

$$\frac{\mathbf{C^{c}}}{\Delta t}(^{(t+\Delta t)}\mathbf{c} - {}^{(t)}\mathbf{c}) = {}^{(t+\Delta t)}\mathbf{f}_{5} \tag{53}$$

The Newton method was used for solving Eqs.52 and 53.

5 Validation

To investigate the validation of the porous model, Simon's one-dimensional poroelastic problem with analytical solution [14, 15] was used. This problem represents the motion of a porous elastic material along the x-axis with a step load at the free top surface. The material properties, initial and boundary conditions are referred to Simon's work [14, 15].

The shape functions used in this one-dimensional problem are isoparametric linear function (Ten elements). Fig.2 shows how the solid and fluid displacements vary with time at x=0.
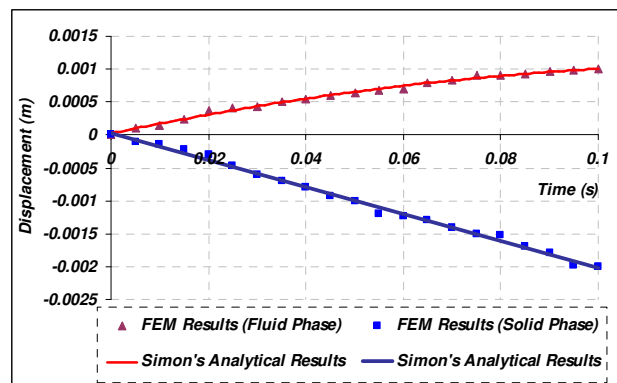

Fig.2: Validation of the model with Simon's work

To validate the mechano-electrochemical phenomenon of charged, hydrated intervertebral disc, a transient free swelling problem was studied using our finite element formulation in compare with Sun's results [19]. Assuming a frictionless lateral boundary, only axial motion is possible and the problem is reduced to a 1-D problem. The shape functions used in this one-dimensional problem are isoparametric linear functions (five elements). Initially tissue sample was at equilibrium with the external bathing solution. At $t=0^{+}$, the concentration of external solution at top decreases linearly according to Fig. 3.
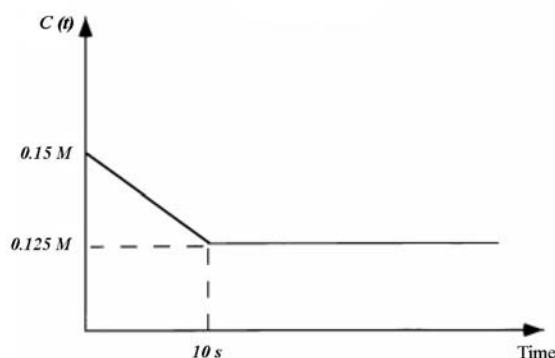

Fig.3: Change of the external solution concentration in the transient free swelling problem

The lowering of concentration causes the tissue to swell to a new equilibrium state. In this free swelling test, the material properties, initial and

boundary conditions are referred to Sun's work [19]. Fig.4 shows the history of the solid displacement at the surface.
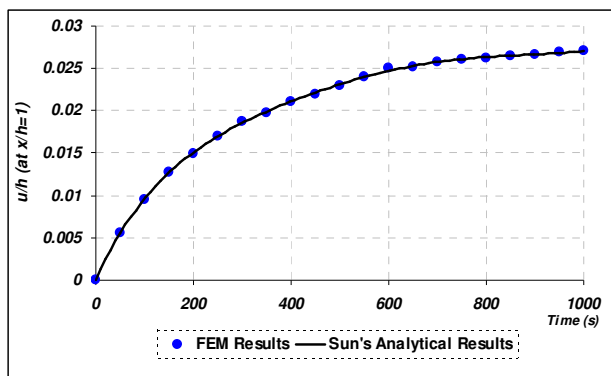

Fig.4: Validation of the model with Sun's work (Free swelling problem)

After validation of the FEM results with analytical solutions, our model was used to simulate the load displacement response as obtained by Drost et al. [27]. That study considered the compression of the canine annulus under chemical and mechanical loading. Using our FEM model, the mentioned experimental test was simulated in following load stages:

(1) Conditioning, $c=0.6$ M, $P=0.08$ MPa
(2) Swelling, $c=0.2$ M, $P=0.08$ MPa
(3) Consolidation, $c=0.2$ M, $P=0.20$ MPa.

Fig.5 shows how the Displacement of annulus fibrosus specimen varies with time and compares theoretical results with experimental data (by Drost et al. [27]).
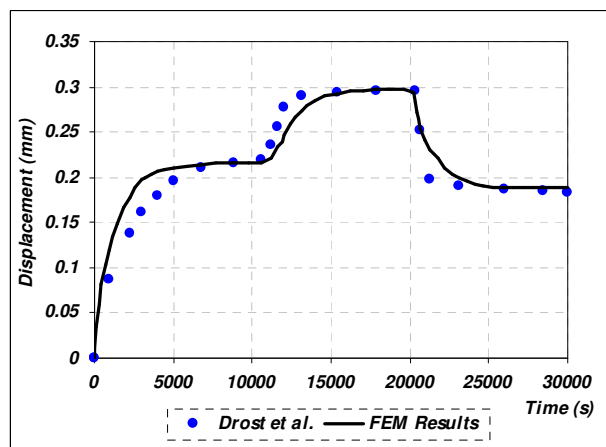

Fig.5: Validation of the model with Drost's experimental data

However, the formulation accuracy and convergence for 1D case were examined and it is clear that the FEM results are in excellent agreement with analytical and experimental works.

Comparison with Simon's [14, 15] and Sun's [19] analytical solutions respectively confirms the validity of our dynamic poroelastic and mechano-electrochemical model. Also agreement of the results of our mathematical model with Drost's [27] experimental data validates our model for application in studying the biomechanics of the intervertebral disc as a hydrated soft tissue.

6 Exemplary Applications of the Model in IVD Tissue Engineering and Related Results

As it mentioned, the main purpose of developing this mathematical model is devoted to study the intervertebral disc mechanobiology during the tissue engineering procedure. On the basis of this infrastructure model we can gain the capability of optimizing the design parameters of porous scaffolds and prediction of the stress distribution in different stages of the tissue engineering. To have a short review of three main exemplary problems, we can mention to the investigation of the role of porosity in scaffold manufacturing, effect of fixed charge density and water content on mechanical response and studying the nutrition criterion in IVD tissue engineering procedure.

6.1 Investigation of the role of porosity

Porosity is the most important morphological parameter of the scaffold which must meet some specific requirements. A high porosity and an adequate pore size are necessary to facilitate cell seeding and diffusion throughout the whole structure of both cells and nutrients. On the other hand it causes very low stiffness and strength which can lead to failure in compare with natural biological tissue. So it is necessary to understand the link between the forces applied to a scaffold and its porosity.

We considered a homogenous two dimensional version of our mathematical model, to analyze a simple sagittal slice of the disc. In the model, we assumed that the bottom surface of the sagittal slice is impermeable, frictionless, insulated, and rigid so that there is no vertical flow. The top edge was loaded with pressure P. In order to compare the difference between different porosity, a long duration (200s) was applied, and the value of P was chosen as a ramp from zero to 2×10^6 Pa in test duration (0~200s). The material properties and requisite parameters were selected as Table 1.

Fig.6 shows the displacement at top with different porosity in mentioned 2-D model. With

increasing time, the differences in the displacement at top between different cases increase. Fig.6 also indicates that the displacement at top increases with increasing the porosity.

On the basis of this exemplary application of our mathematical model and extracting other morphological parameters [28], we gain different range of porosity which is suitable for adjustments of the instrumentation setups for various types of scaffold manufacturing.

Table 1: Material properties and parameters of 2-D model

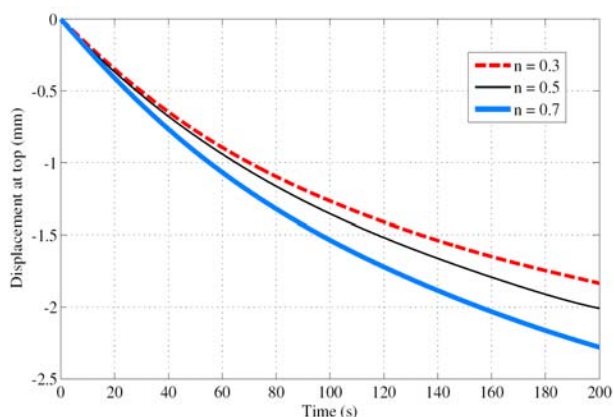| Parameter	Amount and Unit
c	0.2 (M)
B_f	5×10^5 (N/m^2)
E	2×10^6 (N/m^2)
FCD	0.2 (M)
f_{+-}/f_{-+}	1×10^{10} (N-s/m^4)
f_{sf}	1×10^{15} (N-s/m^4)
f_{s+}	1×10^{10} (N-s/m^4)
f_{s-}	1×10^{10} (N-s/m^4)
f_{f+}	5.0039×10^{14} (N-s/m^4)
f_{f-}	7.6021×10^{14} (N-s/m^4)
k	1×10^{-14} (m^4/N-s)
Q	2×10^8 (N/m^2)
R	8.31878×10^3 (m-mN/mol-K)
T	310 (K)
μ_0	0.1 (N-m/Kg)
ρ_f	1000 (Kg/m^3)
ρ_s	1026 (Kg/m^3)
ζ_w	0.75
φ	0.5
υ	0.48

Fig.6: Displacement at top with different porosity

6.2 Effect of fixed charge density and water content on mechanical response of engineered tissue

Due to the coupling of mechanical and electrical effects, the measured hydraulic permeability of charged tissues, such as intervertebral disc tissues, also depends on the electrical current flow [29-32]. So it is important to investigate the effect of fixed charge density and water content in a natural intervertebral disc to optimize the related design parameters in tissue engineering procedure.

As we predicted, our infrastructure model is capable for this study. A homogenous two dimensional version of this mathematical model, can analyze the effect of fixed charge density in a simple sagittal slice of the disc. For the compression creep problem, σ_0=10 KPa was applied to the 2-D intervertebral disc model. The related parameters, initial and boundary conditions were selected as Table 2.

Table 2: Material properties and parameters of 2-D model, Initial and boundary conditions

Parameter	Amount and Unit
c	0.2 (M)
B_f	5×10^5 (N/m^2)
E	2×10^6 (N/m^2)
f_{+-}/f_{-+}	1×10^{10} (N-s/m^4)
f_{sf}	1×10^{15} (N-s/m^4)
f_{s+}	1×10^{10} (N-s/m^4)
f_{s-}	1×10^{10} (N-s/m^4)
f_{f+}	5.0039×10^{14} (N-s/m^4)
f_{f-}	7.6021×10^{14} (N-s/m^4)
k	1×10^{-14} (m^4/N-s)
n	0.5
Q	2×10^8 (N/m^2)
R	8.31878×10^3 (m-mN/mol-K)
T	310 (K)
μ_0	0.1 (N-m/Kg)
ρ_f	1000 (Kg/m^3)
ρ_s	1026 (Kg/m^3)
ζ_w	0.8
φ	0.5
υ	0.48
Initial Condition	
At t=0: u=0	
Boundary Condition	
At Y=0: u=0	

The effect of fixed charge density on creep deformation was investigated with three different amounts (FCD= 0.1, 0.2 and 0.3) and plotted in
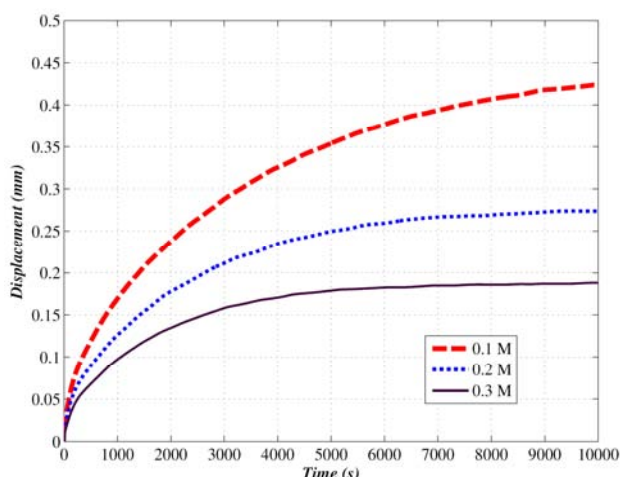
Fig.7.

Fig.7: Effect of fixed charge density on the creep behavior

In next step, by selecting the parameters and conditions according to Table 2 and fixed charge density equal to 0.2 M, the effect of water content on creep deformation was investigated with three different amounts (ζ_w= 0.7, 0.8 and 0.9) and plotted in Fig.8.
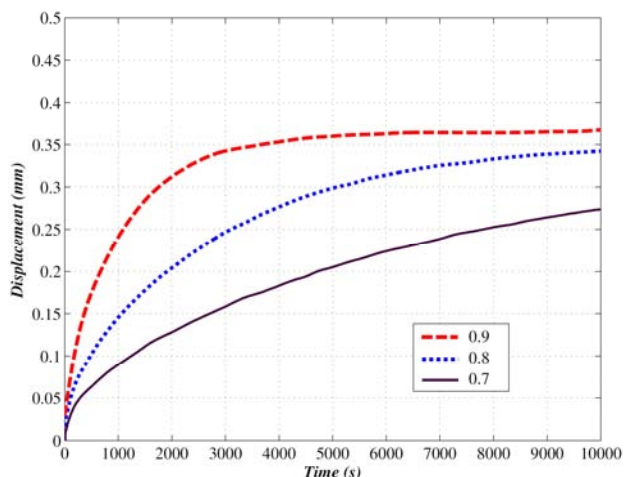

Fig.8: Effect of water content on the creep behavior

Fig.7 shows that increasing the fixed charge density lead to decreasing the displacement. It means that with increasing the fixed charge density, the tissue becomes stiffer. Fig.8 shows that with increasing water content, the time to reach creep equilibrium decreases. However, changes in water content do not affect the equilibrium strain significantly.

6.3 Investigation of the nutrition criterion in IVD tissue engineering procedure

The disc is regarded as the largest avascular structure in the body and the cells of adult lumbar discs may be up to 8mm away from the nearest blood supply. Diffusion of solutes across concentration gradients is the principal mechanism by which the disc receives its nutrition. So it is so important to study the biomechanics of this phenomenon in tissue engineering.

For determination of the effect of mechanical loading regimes in nutrition of the intervertebral disc metabolism, we calculated the influence of the cycle length and amplitude of the dynamic loading in a two-dimensional model. Similarly, we considered a simple homogenous sagittal model, and the endplates and vertebral bodies were assumed to be incompressible. The dynamic loading was chosen as square wave to represent loads experienced by the intervertebral disc for a person who is alternating between activity and rest [33, 34]. So the dynamic loading was defined as a square wave with amplitude of 1MPa. Also the material properties and requisite parameters were selected as Table 1.

In this case first we derived two fluid exchange factors. The first one is the volume of fluid exchange per cycle, which represents the volume of disc included in the fluid exchange region. So we calculated this factor by dividing the final total volume of fluid exchange by the total number of cycle which occurred during the dynamic loading simulation. The second one is the volume of fluid exchange between the disc and the surrounding media per unit time. So we calculated this factor by dividing the final total volume of fluid exchange by the total duration of the dynamic loading simulation.

After definition of these two factors, we calculated the results of our mathematical mode by changing cycle length from zero to 12 hours in dynamic loading. Fig.9 shows how these factors vary with cycle length in a normalized scale.
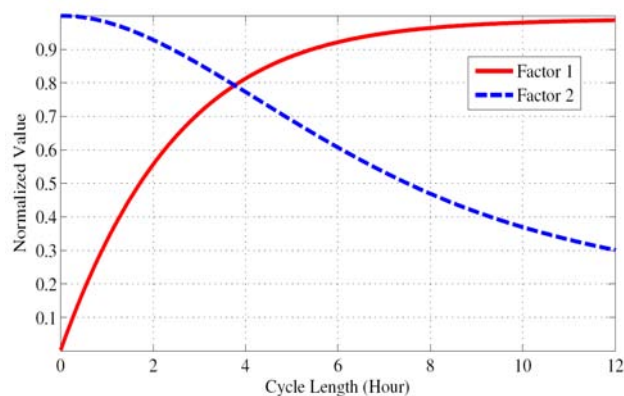

Fig.9: Variations of the Factor 1 (the volume of fluid exchange per loading cycle) Factor 2 (the volume of fluid exchange per unit time) with cycle length.

To derive a criterion in fluid transport study, we maximized these two mentioned fluid factors and normalized it to define a nutrition index. Fig.10 shows how this criterion changes regarding to different cycle lengths.
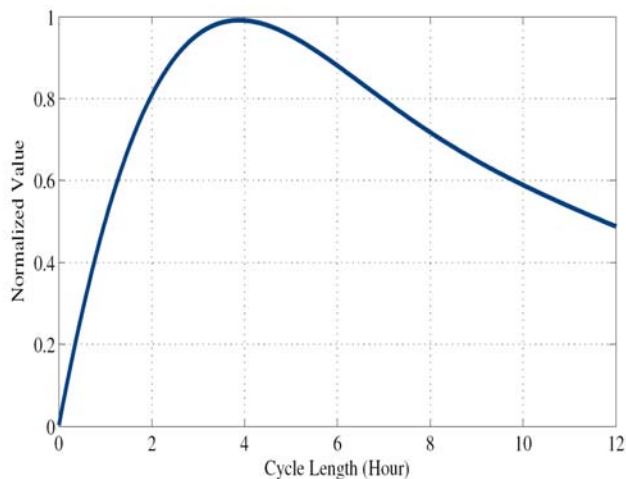

Fig.10: Variations of the nutrition criterion with cycle length

The results show that as the cycle length increase, the volume of fluid exchange per cycle increases but in opposite the volume of fluid exchange per unit time decreases. By maximizing these results, the nutrition criterion shows a peak for a cycle length approximately equal to 4 hours. So our model shows that the optimum balance of these factors occurs for an alternating spinal load every 2 hours.

In next step, we repeated these results for four different amplitudes of loading. Fig.11 shows the comparison of nutrition criterion in these different amplitudes.
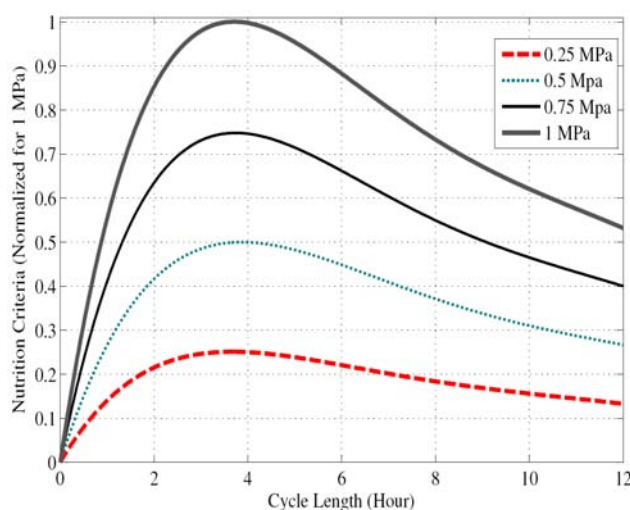

Fig.11: Comparison of the nutrition criterion in different rang of compressive loading with cycle length

As it was predicted, decreasing the amplitude decreases the nutrition criteria but does not change the trend of normalized results regarding to the cycle length. So this model suggests that increasing the amplitude of loading has an effective response on disc nutrition supply. However, an optimum magnitude of compressive loading in tissue engineering would be also constrained by other biological factors which should be included in future analyses.

7 Conclusion

One of the major challenges in the intervertebral disc tissue engineering is to recreate, in vitro, the physiological environment for optimal culturing of cells seeded in scaffolds constructs. So it is necessary to understand the link between the forces applied to this soft tissue and its biological response. Based on the importance of considering the inertia terms and electro chemical behaviour in modeling the biomechanical responses of the tissue engineering procedure, this novel mathematical model is constructed. The standard Galerkin weighted residual method was used for providing numerical solution to this problem (which is intractable to analytic solution) and then implicit time integration schemes are applied to solve the nonlinear equations.

Our model was verified by comparison of the derived finite element results for one dimensional model with analytical solution and also experimental data. Comparison with Simon's [14, 15] and Sun's [19] analytical solutions respectively confirms the validity of our dynamic poroelastic and mechano-electrochemical model. Also agreement of the results of our mathematical model with Drost's [27] experimental data validates our model for application in studying the biomechanics of the intervertebral disc as a hydrated soft tissue. No locking and spurious modes such as checkerboard phenomenon are found in the calculation. Through these sample cases, it is shown that our finite element model is capable of solving the complex triphasic problems of charged hydrated soft tissues under different types of mechanical, electrical and physicochemical loading conditions.

Based on this mathematical model, as examples, we investigated the role of porosity in scaffold manufacturing, effect of fixed charge density and water content on mechanical response and also the nutrition criterion in intervertebral disc tissue engineering procedure.

Different results of this infrastructure model can

lead in logical algorithms in intervertebral disc tissue engineering in order to reduce trial and errors. However, designing an optimum algorithm in this case would be also constrained by other biological factors and it is the reason that we devote our future works to develop this model with combination of the biological experiments in details. We will trace our future researches in order to gain a complete understanding of IVD mechanobiology and the procedure of the tissue differentiation to finalize the setups of the instrumentations for tissue engineering.

8 Appendix

The momentum conservation law for the porous solid in the absence of body force has been derived in Eulerian form by Simon et al. [21] as Eq.54.

$$(1-n)\nabla p + R_s \dot{\mathbf{w}} - \nabla p^c + \mathbf{L}^T(\boldsymbol{\sigma}') = \rho_s(1-n)\ddot{\mathbf{u}} \tag{54}$$

Where:

$$p^c = B_f \zeta_w - \rho_f \mu_0^w + RT\phi(2c + FCD) \tag{55}$$

$$\mathbf{L}^T = \begin{bmatrix} \dfrac{\partial}{\partial x_1} & 0 & 0 & \dfrac{\partial}{\partial x_2} & 0 & \dfrac{\partial}{\partial x_3} \\ 0 & \dfrac{\partial}{\partial x_2} & 0 & \dfrac{\partial}{\partial x_1} & \dfrac{\partial}{\partial x_3} & 0 \\ 0 & 0 & \dfrac{\partial}{\partial x_3} & 0 & \dfrac{\partial}{\partial x_2} & \dfrac{\partial}{\partial x_1} \end{bmatrix} \tag{56}$$

$$\nabla = \begin{bmatrix} \dfrac{\partial}{\partial x_1} \\ \dfrac{\partial}{\partial x_2} \\ \dfrac{\partial}{\partial x_3} \end{bmatrix} \tag{57}$$

The momentum conservation law for the pore fluid in the absence of body force has been formed by Simon et al. (in Eulerian form) [21] as Eq.58 (According to the Darcy theory)

$$n\nabla p - R_s \dot{\mathbf{w}} + \nabla p^c = n\rho_{fluid}\ddot{\mathbf{u}} + n\rho_{fluid}\ddot{\mathbf{w}} \tag{58}$$

Multiplying Eq.58 by $\dfrac{1}{n}$ yields a generalized Darcy law as Eq.59

$$\nabla p - \frac{n}{k}\dot{\mathbf{w}} + \frac{\nabla p^c}{n} = \rho_{fluid}\ddot{\mathbf{u}} + \rho_{fluid}\ddot{\mathbf{w}} \tag{59}$$

Where,

$$k = \frac{n^2}{R_s} \tag{60}$$

From Eq.54 and 58, we can derive Eq.61

$$\nabla p + \mathbf{L}^T(\boldsymbol{\sigma}') = \rho\ddot{\mathbf{u}} + n\rho_{fluid}\ddot{\mathbf{w}} \tag{61}$$

We can rewrite the Eq.61 as Eq.62 by means of Eqs.63.

$$\mathbf{L}^T\boldsymbol{\sigma} = \rho\ddot{\mathbf{u}} + n\rho_{fluid}\ddot{\mathbf{w}} \tag{62}$$

$$\boldsymbol{\sigma} = \boldsymbol{\sigma}' + \mathbf{m}p \tag{63}$$

Where,

$$\mathbf{m} = \begin{bmatrix} 1 \\ 1 \\ 1 \\ 0 \\ 0 \\ 0 \end{bmatrix} \tag{64}$$

In Lagrangian form we can rewrite the Eq.62 and 59 as Eqs.65 and 66

$$\mathbf{L}_0^T(\mathbf{T}) = \rho\ddot{\mathbf{u}} + n\rho_{fluid}(J^{-1}\mathbf{F})\ddot{\mathbf{w}} \tag{65}$$

$$\mathbf{F}^{-1}\cdot\nabla_0 p + \mathbf{F}^{-1}\cdot\nabla_0(\frac{p^c}{n}) - \frac{n}{k}(J^{-1}\mathbf{F}^T)\dot{\mathbf{w}}$$
$$= \rho_{fluid}\ddot{\mathbf{u}} + \rho_{fluid}(J^{-1}\mathbf{F}^T)\ddot{\mathbf{w}} \tag{66}$$

Where,

$$\mathbf{L}_0^T = \begin{bmatrix} \dfrac{\partial}{\partial X_1} & 0 & 0 & \dfrac{\partial}{\partial X_2} & 0 & \dfrac{\partial}{\partial X_3} \\ 0 & \dfrac{\partial}{\partial X_2} & 0 & \dfrac{\partial}{\partial X_1} & \dfrac{\partial}{\partial X_3} & 0 \\ 0 & 0 & \dfrac{\partial}{\partial X_3} & 0 & \dfrac{\partial}{\partial X_2} & \dfrac{\partial}{\partial X_1} \end{bmatrix} \tag{67}$$

$$\nabla_0 = \begin{bmatrix} \dfrac{\partial}{\partial X_1} \\ \dfrac{\partial}{\partial X_2} \\ \dfrac{\partial}{\partial X_3} \end{bmatrix} \tag{68}$$

$$\mathbf{T} = \mathbf{F}^{-1}\cdot\boldsymbol{\sigma} \tag{69}$$

$$J = \det\left|\frac{\partial x}{\partial X}\right| \tag{70}$$

Multiplying Eq.66 by $\mathbf{F}$ yields Eq.71

$$\nabla_0(p + \frac{p^c}{n}) - \frac{n}{k}\dot{\mathbf{w}} = \rho_{fluid}\mathbf{F} \cdot \ddot{\mathbf{u}} \qquad (71)$$
$$+ \rho_{fluid}(J^{-1}\mathbf{F} \cdot \mathbf{F}^T) \cdot \ddot{\mathbf{w}}$$

Where the permeability in lagrangian form (**k**) is as Eq.72,

$$\mathbf{k} = kJ\mathbf{F}^{-T} \cdot \mathbf{F}^{-1} = k\mathbf{I} \qquad (72)$$

Eq.65 and 71 in tensor form can be written as Eq.73 and 74 which were mentioned directly in main part of the paper:

$$\frac{\partial T_{ji}}{\partial X_j} - \rho\ddot{u}_i - n\rho_f(J^{-1}\frac{\partial x_i}{\partial X_j})\ddot{w}_j = 0 \qquad (73)$$

$$\frac{\partial(p + \frac{p^c}{n})}{\partial X_i} - \frac{n}{k}\dot{w}_j - \rho_f\frac{\partial x_j}{\partial X_i}\ddot{u}_j \qquad (74)$$
$$- \rho_f(J^{-1}\frac{\partial x_k}{\partial X_i}\frac{\partial x_k}{\partial X_j})\ddot{w}_j = 0$$

Nomenclature:

c Concentration of the ion phase

B_f Coupling coefficient in the chemical potential

E   Strain Tensor

E   Modulus of elasticity

F   Deformation gradient

FCD   Fixed charge density

f_+/f_+ Frictional coefficients between positive and negative ions

f_{+sf} Summation of the frictional coefficients between positive ion and solid phase and the frictional coefficients between positive ion and fluid phase

f_{-sf} Summation of the frictional coefficients between negative ion and solid phase and the frictional coefficients between negative ion and fluid phase

J Jacobean Matrix

$\mathbf{J}^+ / \mathbf{J}^-$ Positive / negative ion flux

k Permeability

K_s / K_f Bulk module for the solid / fluid phases

k   Permeability in Lagrangian form

K   Stiffness matrix

n Porosity

N^i Shape functions

P Fluid pressure

p^c Pressure due to the chemical potential

R Universal gas constant

R_s Isotropic resistivity

T   Stress Tensor

T Absolute temperature

t_i Pressure at the boundary

u   Displacement of solid

$\mathbf{v}^\alpha$ Velocity of α component

w   Relative displacement of fluid

μ^+/μ^- Electrochemical potentials for Cation / Anion

μ_0 Reference chemical potential

ρ_α Mass density of α component

ζ_w Variation of water content

φ Osmotic coefficient

υ Poisson ratio

∇ Gradient operator

References:

[1] R.A. Deyo, Y.J. Tsui-Wu, Descriptive epidemiology of low back pain and its related medical care in the United States, *Spine*, Vol.12, 1987, pp.264-268.

[2] T. Yasuma, S. Koh, T. Okamura, Y. Yamauchi, Histological changes in aging lumbar intervertebral discs Their role in protrusions and prolapses, *The Journal of Bone and Joint Surgery*, Vol.72, 1990, pp.220-229.

[3] M.A. Adams, P. Dolan, "Spine biomechanics", *Journal of Biomechanics*, Vol.38, 2005, pp.1972-1983.

[4] K. Sato, S. Kikuchi, In Vivo intra discal pressure measurement in healthy individuals and patients with ongoing back problem, *Spine*, Vol. 24, 1999, pp. 2468-2474.

[5] H. Mizuno, A. Roy, V. Zaporojan, C. Vacanti, M. Ueda, L. Bonassar, Biomechanical and biochemical characterization of composite tissue-engineered intervertebral discs., *Biomaterials*, Vol.27, 2006, pp.362-370.

[6] A. Lori, A. Setton, Cell mechanics and mechanobiology in the intervertebral disc, *Spine*, Vol.29, 2004, pp.2710-2723.

[7] W. Hutton, W. Elmer, L. Bryce, E. Kozlowska,

S. Boden, M. Kozlowski, Do the intervertebral disc cells respond to different levels of hydrostatic pressure?, *Clinical Biomechanics*, Vol.16, 2001, pp.728-734.

[8] P. Goupille, M. Jayson, J. Valat, A. Freemont, Matrix metalloproteinases: the clue to intervertebral disc degeneration, *Spine*, Vol.23, 1998, pp.1612-1626.

[9] V.C. Mow, S.C. Kuei, W.M. Lai, C.G. Armstrong, Biphasic creep and stress relaxation of articular cartilage: Theory and experiments, *Journal of Biomechanical Engineering*, Vol.102, 1980, pp. 73-84.

[10] R.L. Spilker, J.K. Suh, Formulation and evaluation of a finite element model for the biphasic model of hydrated soft tissue, *Computers & Structures*, Vol.35, No. 4, 1990, pp. 425-439.

[11] J.K. Suh, R.L. Spilker, M.H. Holmes, A penalty finite element analysis for nonlinear mechanics of biphasic hydrated soft tissue under large deformation, *International Journal for Numerical Methods in Engineering*, Vol. 32, 1991, pp. 1411-1439.

[12] J.K. Suh, S. Bai, Finite element formulation of biphasic poroviscoelastic model for articular cartilage, *Journal of Biomechanical Engineering*, Vol.120, 1998, pp.195-201.

[13] J.K. Suh, M.R. DiSilvestro, Biphasic poroviscoelastic behavior of hydrated biological soft tissue, *Journal of Applied Mechanics*, Vol. 66, 1999, pp. 528-535.

[14] B.R. Simon, J.S.S. Wu, M.W. Carlton, J.H. Evans, L.E. Kazarian, Structural models for human spinal motion segments based on a poroelastic view of the intervertebral disc, *Journal of Biomechanical Engineering*, Vol.107, 1985, pp. 327-335.

[15] B.R. Simon, J.S.S. Wu, M.W. Carlton, Poroelastic dynamic structural models of Rhesus spinal motion segments, *Spine*, Vol.10, 1985, pp. 494-507.

[16] Z. Yang, P. Smolinsky, Dynamic finite element modeling of poroviscoelastic soft tissue, *Computer Methods in Biomechanics and Biomedical Engineering*, Vol.9, 2006, pp. 7-16.

[17] W.M. Lai, J.S. Hou and V.C. Mow, A triphasic theory for the swelling and deformation behavior of articular cartilage, *Journal of Biomechanical Engineering*, Vol. 113, 1991, pp. 245-258.

[18] W.Y. Gu, W.M. Lai and V.C. Mow, A mixture theory for charged-hydrated soft tissues containing multi-electrolytes: passive transport and swelling behaviors, *Journal of Biomechanical Engineering*, Vol. 120, 1998, pp. 169-180.

[19] D.N. Sun, W.Y. Gu, X.E. Guo, W.M. Lai, and V.C. Mow, A mixed finite element formulation of Triphasic mechano-electrochemical theory for charged, hydrated biological soft tissues, *International Journal of Numerical Methods in Engineering*, Vol. 45, 1999, pp. 1375-1402.

[20] B.R. Simon, Multiphase poroelastic finite element models for soft tissue structures, *Applied Mechanics Reviews*, Vol. 45, 1992, pp.191-218.

[21] B.R. Simon, , J.P. Liable, Y. Yuan, M.H. Krag, A poroelastic finite element formulation including transport and swelling in soft tissue structures, *Journal of Biomechanical Engineering*, Vol.118, 1996, pp. 1-9.

[22] J.P. Laible, D.S. Pflaster, M.H. Krag, A poroelastic-swelling finite element model with application to the intervertebral disc, *Spine*, Vol.18, 1993, pp. 659-670.

[23] J.C. Iatridis, J.P. Laible, M.H. Krag, Influence of fixed charge density magnitude and distribution on the intervertebral disc: applications of a poroelastic and chemical electric (PEACE) model, *Journal of Biomechanical Engineering*, Vol.125, 2003, pp. 12-24.

[24] M. Nikkhoo, M. Haghpanahi, H. Peirovi, J. Ghanavi, Mathematical model for tissue engineered intervertebral disc as a saturated porous media, *Proceedings of the 3rd WSEAS International Conference on Applied and Theoretical Mechanics*, Spain, December 2007, pp. 197-201.

[25] K.J. Bathe, *Finite Element Procedure*, Prentice Hall, 1995.

[26] D.G. Duffy, *Advanced Engineering Mathematics with MATLAB*, Chapman and Hall/CRC, 2003.

[27] M.R. Drost, P. Willems, H. Snijders, J.M. Huyghe, J.D. Janssen, A. Huson, Confined Compression of Canine Annulus Fibrosus Under Chemical and Mechanical Loads, *Journal of Biomechanical Engineering*, Vol.117, 1995, pp. 390-396.

[28] M. Haghpanahi, S. Miramini, Extraction of Morphological Parameters of Tissue Engineering Scaffolds using Two-Point Correlation Function, *Proceedings of the 6th IASTED International Conference on Biomedical Engineering*, Austria, February 2008.

[29] S. R. Bibby, J. C. Fairbank, M. R. Urban, J. P. Urban, Cell viability in scoliotic discs in relation to disc deformity and nutrient levels, *Spine*, Vol.27, 2002, pp.2220–2228.

[30] W. Y. Gu, M. A. Justiz, H. Yao, Electrical conductivity of lumbar annulus fibrosis: Effects of

porosity and fixed charge density, *Spine*, Vol.27, 2002, pp.2390-2395.

[31] W. Y. Gu, M. A. Justiz, Apparatus for measuring the swelling dependent electrical conductivity of charged hydrated soft tissues, *Journal of Biomechanical Engineering*, Vol.124, 2002, pp.790-793.

[32] J. M. Huyghe, J. D. Janssen, Quadriphasic mechanics of swelling incompressible porous media, *International Journal of Engineering Science*, Vol.35, 1997, pp.793–802.

[33] T. Matsumoto, M. Kawakami, K. Kuribayashi, T. Takenaka, T. Tamaki, Cyclic mechanical stretch stress increases the growth rate and collagen synthesis of nucleus pulposus cells in vitro, *Spine*, Vol.24, 1999, pp.315-319.

[34] K. Wenger, A. Woods, A. Holecek, E. Eckstein, J. Robertson, K. Hasty, Matrix remodeling expression in annulus cells subjected to increased compressive load, *Spine*, Vol.30, 2005, pp.1122-1126.